Biochimica et Biophysica Acta 1838 (2014) 2115–2126

Contents lists available at ScienceDirect

Biochimica et Biophysica Acta

journal homepage: www.elsevier.com/locate/bbamem

Effects of sphingomyelin/ceramide ratio on the permeability and microstructure of model stratum corneum lipid membranes

Petra Pullmannová [a,*], Klára Staňková [a], Markéta Pospíšilová [a], Barbora Školová [a], Jarmila Zbytovská [b], Kateřina Vávrová [a]

[a] Skin Barrier Research Group, Charles University in Prague, Faculty of Pharmacy, Heyrovského 1203, 500 05 Hradec Králové, Czech Republic
[b] Institute of Chemical Technology Prague, Technická 5, 166 28 Prague, Czech Republic

ARTICLE INFO

Article history:
Received 4 February 2014
Received in revised form 10 April 2014
Accepted 3 May 2014
Available online 11 May 2014

Keywords:
Sphingomyelin
Ceramide
Stratum corneum model
Lipid membrane
Permeability
X-ray diffraction

ABSTRACT

The conversion of sphingomyelin (SM) to a ceramide (Cer) by acid sphingomyelinase (aSMase) is an important event in skin barrier development. A deficiency in aSMase in diseases such as Niemann–Pick disease and atopic dermatitis coincides with impaired skin barrier recovery after disruption. We studied how an increased SM/Cer ratio influences the barrier function and microstructure of model stratum corneum (SC) lipid membranes. In the membranes composed of isolated human SC Cer (hCer)/cholesterol/free fatty acids/cholesteryl sulfate, partial or full replacement of hCer by SM increased water loss. Partial replacement of 25% and 50% of hCer by SM also increased the membrane permeability to theophylline and alternating electric current, while a higher SM content either did not alter or even decreased the membrane permeability. In contrast, in a simple membrane model with only one type of Cer (nonhydroxyacyl sphingosine, CerNS), an increased SM/Cer ratio provided a similar or better barrier against the permeation of various markers. X-ray powder diffraction revealed that the replacement of hCer by SM interferes with the formation of the long periodicity lamellar phase with a repeat distance of d = 12.7 nm. Our results suggest that SM-to-Cer processing in the human epidermis is essential for preventing excessive water loss, while the permeability barrier to exogenous compounds is less sensitive to the presence of sphingomyelin.

1. Introduction

Lipids filling the intercellular space of the stratum corneum (SC) are essential for the function of the skin barrier in terrestrial mammals. The highly ordered skin barrier lipids include three main groups of hydrophobic compounds – ceramides (Cer), free fatty acids (FFA) and cholesterol (Chol) – in approximately equimolar fractions, with a minor amount of cholesteryl sulfate (CholS) [1]. Cer (*i.e.*, *N*-acylsphingosines) belong to the sphingolipids. There are at least 12 classes of Cer occurring in the human SC, including the very long acylCer (EO-class Cer), which contain 30–34C acyls with linoleic acid ester-linked to ω-hydroxyl [2,3]. AcylCer play a crucial role in the homeostasis of the permeability barrier [4–6]. The presence of acylCer is necessary for the formation of the so-called long periodicity lamellar phase (LPP, repeat distance of approximately 13 nm) that is typical for the human SC lipid matrix [7–9]. The lamellar structure of SC was at first visualized by freeze-fracture electron microscopy [10,11]. X-ray diffraction confirmed that the intercellular domains of murine SC form the lamellar phase with a repeat distance ~13 nm [12]. Since the 1980s, artificial lipid systems started to be systematically studied with the aim to propose the molecular arrangement of the lipid structures in the epidermal barrier [13].

In SC intercellular domains, hydrolytic enzymes release Cer from their polar precursors: glucosylceramides and sphingomyelins (SM). This processing is crucial for homeostasis of the epidermal barrier but is likely not complete; the total content of polar lipids was estimated to be between 2.3 and 5.2% (by weight) of healthy human SC lipids [14,15]. However, the amount of the individual precursors, glucosylceramides and SM, has not been reported.

In this work, we focused on the SM-to-Cer pathway. SM are converted to Cer (type NS or AS) and phosphocholine by acid sphingomyelinase (aSMase) (Fig. 1). These SM-derived Cer are indispensable for skin barrier function. For example, delayed recovery of the skin permeability barrier has been found in patients with Niemann–Pick disease, which is caused by a mutation in the SMPD1 gene that results in a severe decrease in aSMase activity [16]. Reduced enzymatic activity of aSMase

Abbreviations: aSMase, acid sphingomyelinase; acylCer, ω-O-acyl ceramide/s; Cer, ceramide/s; AD, atopic dermatitis; Chol, cholesterol from lanolin; FFA, free fatty acid/s; IND, indomethacin; HPTLC, high performance thin layer chromatography; hCer, ceramides of the human stratum corneum; LPP, long periodicity phase; PBS, phosphate-buffered saline; SPP, short periodicity phase; CholS, sodium cholesteryl sulfate; SM, sphingomyelin; eSM, sphingomyelin, chicken egg; bmSM, sphingomyelin, bovine milk; SEM, standard error of mean; SC, stratum corneum; TH, theophylline, anhydrous; TLC, thin layer chromatography

* Corresponding author at: Department of Inorganic and Organic Chemistry, Charles University in Prague, Faculty of Pharmacy, Heyrovského 1203, 500 05 Hradec Králové, Czech Republic.
E-mail address: pullmanp@faf.cuni.cz (P. Pullmannová).

http://dx.doi.org/10.1016/j.bbamem.2014.05.001
0005-2736/

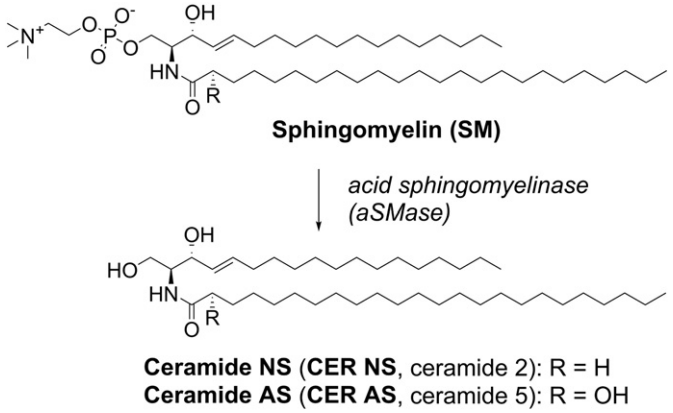

Fig. 1. Conversion of sphingomyelin (SM) to the ceramides (Cer) NS and AS — schematic representation.

has also been reported in atopic dermatitis (AD) patients and was proposed to be related to the decreased amount of Cer in SC lipids [17]. However, the role of aSMase in the development of skin barrier abnormalities remains unclear. In particular, there is also a report describing an increased amount of epidermal SMase in lesional human AD skin [18]. Evaluating the effect of decreased aSMase activity is also complicated by the abnormally expressed SM deacylase in atopic patients, which cleaves SM to FFA and sphingosylphosphorylcholine [19,20].

To provide greater mechanistic insight into the importance of this Cer-generating pathway, Schmuth et al. applied an aSMase inhibitor to the skin of hairless mice. The aSMase inhibition induced a 4-fold accumulation of SM in the murine SC after an acute barrier disruption (from 0.3% to 1.2% of the total SC lipid mass). The changed SM/Cer ratio was suggested to be responsible for the altered skin barrier function [16]. Similarly, the suppressed β-glucocerebrosidase enzymatic activity was followed by an accumulation of Cer precursors glucosylceramides in the SC [21]. However, a direct effect of SM on the permeability of SC has not been demonstrated.

The purpose of our work was to study how an increased SM/Cer ratio influences the permeability and biophysics of membranes composed of SM/Cer/FFA/Chol/CholS that model the SC intercellular lipid lamellae. We prepared lipid membranes containing either only one type of Cer — nonhydroxyacyl sphingosine (CerNS) or the full spectrum of isolated human SC Cer (hCer). To determine how SM accumulation affects the SC lipid barrier, various fractions of Cer (either CerNS or hCer) were replaced by equimolar SM. The barrier properties of these model membranes were studied in permeation experiments using four permeability markers, including relative water loss, the steady-state fluxes of theophylline and indomethacin and the electrical impedance. Furthermore, we used small- and wide-angle X-ray powder diffraction to provide insight into the microstructure of SC models with and without SM.

2. Material and methods

2.1. Chemicals and material

N-tetracosanoyl-D-*erythro*-sphingosine (CerNS), *N*-(2′-(*R*)-hydroxytetracosanoyl)-D-*erythro*-sphingosine (CerAS), sphingomyelin from chicken egg (eSM) and sphingomyelin from bovine milk (bmSM) were purchased from Avanti Polar Lipids (Alabaster, USA). *N*-tetracosanoyl-D-*erytho*-phytosphingosine (CerNP) was synthesized according to the previously described method [22]. Cholesterol from lanolin (Chol), sodium cholesteryl sulfate (CholS), hexadecanoic acid, octadecanoic acid, eicosanoic acid, docosanoic acid, tetracosanoic acid, theophylline, anhydrous (TH), indomethacin (IND), gentamicin sulfate from Micromonospora purpurea, trypsin from porcine pancreas (1:250 powder, 1500 BAEE units/mg solid), sodium phosphate dibasic dodecahydrate, propylene glycol and solvents were purchased from Sigma-Aldrich Chemie Gmbh (Schnelldorf, Germany). All solvents were analytical or HPLC grade. *N*-(2-hydroxy octadecanoyl)-phytosphingosine 94.8% (CerAP) was purchased from Evonik Industries AG (Essen, Germany). Sodium hydroxide, sodium chloride, potassium chloride and sodium phosphate monobasic dihydrate were supplied from Lachema (Neratovice, Czech Republic). Hydrochloric acid was purchased from Penta (Prague, Czech Republic). The chemicals were analytical grade and used without further purification. The silica gel 60 (230–400 mesh) for column chromatography, HPTLC 20 × 10 cm glass plates (silica gel 60) and TLC plates (silica gel 60 F 254, aluminum back) were from Merck (Darmstadt, Germany). Nuclepore™ track-etched polycarbonate membranes of 0.015 μm pore size were from Whatman (Kent, Maidstone, United Kingdom). The aqueous solutions were prepared with Millipore water.

2.2. Skin

Human abdominal or breast skin from Caucasian female patients (n = 6), who had undergone plastic surgery, was provided by the University Hospital Hradec Králové, Clinics of Plastic Surgery. The procedure was approved by the Ethics Committee of the University Hospital Hradec Králové, Czech Republic (No. 200609 S09P) and was conducted according to the Declaration of Helsinki Principles. Within 6 h of the surgery, residual subcutaneous fat was removed from the skin by a scalpel. The skin was gently wiped with a tissue paper soaked in acetone to remove skin sebum and contaminating subcutaneous fat. The skin fragments were washed in phosphate-buffered saline at pH 7.4 (PBS solution, 10 mM buffer adjusted to 150 mM ionic strength containing 137 mM NaCl, 8 mM $Na_2HPO_4.12H_2O$, 2 mM $NaH_2PO_4.2H_2O$ and 2.7 mM KCl) with 50 mg/L gentamicin for preservation and were stored at −20 °C.

2.3. Isolation of human SC lipids

The SC was isolated using a modified procedure described by Kligman and Christophers [23]. Frozen human skin was slowly thawed and subsequently immersed in 60 °C Millipore water for 30 s. The epidermis was peeled off using tweezers. Then, the epidermis was incubated overnight with the basal layer down in a solution of 0.5% trypsin in PBS at pH 7.4 and 32 °C. The residual epidermal cells were gently removed from the SC using cotton swabs. The SC was washed several times in Millipore water and was washed once briefly in acetone. Afterward, the SC was dried in vacuum over P_4O_{10} and solid paraffin in a desiccator and stored in nitrogen environment at −20 °C.

The SC lipids were extracted from pooled SC of 6 objects by a modified method of Bligh and Dyer [24] with a series of chloroform:methanol mixtures (2:1, 1:1, and 1:2 v/v) for 2 h each. The solvent from the combined extracts was removed using a rotary vacuum evaporator.

2.4. Isolation of human SC Cer (hCer)

The obtained human SC lipids were redissolved in a suitable volume of chloroform–methanol (2:1 v/v) and applied to a silica gel column (Silicagel 60, Merck, Darmstadt, Germany). Similar separation of hCer by column chromatography was described previously by Bouwstra et al. [25]. We used a simpler mobile phase composition: the SC lipid classes were eluted sequentially using gradient elution with solvent mixtures (v/v) in the following sequence: chloroform–acetic acid 99:1 and then chloroform–methanol in ratios of 100:1, 50:1, 10:1, 3:1, 2:1, 1:1 and 1:2. The lipid composition of the individual fractions was established by one-dimensional thin layer chromatography that was run in parallel with standards. To ensure complete separation of the least polar Cer and FFA, the separation of these fractions was repeated.

The fractions containing the eluted Cer were collected, and the solvent was removed using a rotary vacuum evaporator and then in high vacuum over P_4O_{10} and solid paraffin. The isolated hCer were stored under nitrogen at −20 °C.

2.5. High performance thin layer chromatography (HPTLC) analysis of hCer

Qualitative and quantitative analysis of the isolated hCer was performed using high performance thin layer chromatography (HPTLC) according to Bleck et al. [26] and Vavrova et al. [27] with small modifications. The HPTLC glass plate (silica gel 60, Merck, Darmstadt, Germany) was washed with 2:1 chloroform–methanol (v/v), dried and equilibrated at 120 °C for 30 min in a drying oven before use. hCer were dissolved at a concentration of 0.5 mg/mL in 2:1 chloroform–methanol, and the standards were dissolved at a concentration of 1 mg/mL in 2:1 chloroform–methanol (v/v). The samples and standards were sprayed on an HPTLC glass plate under a stream of nitrogen using Linomat V (Camag, Muttenz, Switzerland). The standards were applied to an HPTLC plate together with the analyzed samples to generate calibration curves from 10 μg to 0.1 μg. The HPTLC plate was developed twice with 190:9:1.5 chloroform–methanol–acetic acid (v/v/v) in a solvent-saturated horizontal developing chamber (Camag, Muttenz, Switzerland). The dried plate was immersed in an aqueous solution of 10% $CuSO_4$, 8% H_3PO_4 (v/v), and 5% methanol for 10 s and then charred in a drying oven at 160 °C for 30 min.

A small portion of the hCer was hydrolyzed with 1:9 10 M NaOH–methanol at 60 °C for 1 h. Afterward, the solution was adjusted to pH 4 with 2 M HCl and extracted twice with chloroform. The chloroform layer was concentrated under a stream of nitrogen. The lipids were dried in vacuum over P_4O_{10} and solid paraffin in a desiccator. The hydrolyzed Cer were applied to the HPTLC plate in the same manner as described above. The hydrolysis indicated the presence of acylCer in the hCer fraction because the bands belonging to the acylCer were absent from the sequence of the hydrolyzed hCer.

The (semi)quantification was conducted using densitometry with a TLC Scanner 3 (Camag, Muttenz, Switzerland) at a wavelength of 350 nm. The peak areas were integrated and quantified using CATS software (Camag, Muttenz, Switzerland). The following standards were used to quantify the results: CerNS for the Cer classes NS and EOS; CerNP for NP, EOP and EOH; CerAS for AS, AH and NH; and CerAP for AP.

2.6. Preparation of model SC membranes composed of SM/CerNS/Chol/FFA/CholS and SM/hCer/Chol/FFA/CholS

Free fatty acids (FFA) were mixed in a molar % that corresponds to the native composition of human skin FFA: 1.8% hexadecanoic acid, 4.0% octadecanoic acid, 7.6% eicosanoic acid, 47.8% docosanoic acid and 38.8% tetracosanoic acid [28]. The membranes for modeling SC lipids were prepared as equimolar mixtures of CerNS or hCer, Chol and FFA with the addition of 5 wt.% CholS. The membranes for modeling the altered skin metabolism of SM were prepared by replacing 25, 50, 75 and 100 molar % of Cer (either CerNS or hCer) with SM, either from bovine milk (bmSM) or chicken egg (eSM). The lipid mixtures were dissolved in 2:1 hexane/96% ethanol (v/v) at 4.5 mg/mL, except for the mixture containing hCer, which created a suspension. Because our attempts to dissolve hCer completely by using more solvent or altering its composition did not succeed, the suspension was homogenized using an ultrasound bath and was used in the same manner as the lipid mixture solutions. We used hexane/ethanol solvent because the supporting polycarbonate filters are chemically incompatible with chloroform.

Nuclepore polycarbonate filters were washed in 2:1 hexane/96% ethanol, dried and mounted in a steel holder with a hole of 1 cm diameter, which exposed 0.79 cm^2 of the polycarbonate filter. The lipid solutions (3 × 100 μL per 1 cm^2) were sprayed on the polycarbonate filters under a stream of nitrogen using a Linomat V (Camag, Muttenz, Switzerland) equipped with additional y-axis movement [28] at a flow rate of 10.2 μL/min onto a 10 × 10 mm square. The amount of lipids used per 1 cm^2 was 1.35 mg. The prepared lipid membranes were dried in vacuum over P_4O_{10} and solid paraffin in a desiccator. Before use, the lipid membranes were heated to 90 °C, equilibrated at this temperature for 10 min and slowly (~3 h) cooled down to 32 °C. Afterwards, the membranes were incubated at 32 °C for at least 24 h.

2.7. Donor samples for permeation studies

Donor samples were prepared as 5% (w/w) suspensions of theophylline (TH) or 2% (w/w) suspensions of indomethacin (IND) in Millipore water-60% propylene glycol (v/v). The samples were stirred for 5 min and then allowed to equilibrate at 32 °C for 12 h. Before the application to the lipid membranes, the samples were resuspended. The concentrations were selected so that all the samples were saturated with the pertinent model drug to maintain the same thermodynamic activity throughout the experiments.

2.8. Permeation experiments

The permeability of the model lipid membranes was evaluated using Franz-type diffusion cells with an available diffusion area of 0.5 cm^2 and an acceptor volume of approximately 6.5 mL. The membranes were mounted into the Franz-type diffusion cells with the lipid film facing the donor compartment using Teflon holders. The acceptor compartment of the cell was filled with PBS solution at pH 7.4 containing 50 mg/L gentamicin. The acceptor phase was stirred at 32 °C; the precise volume was measured for each cell individually and was included in the calculation. After a 12-h equilibration at 32 °C, the relative water loss and electrical impedance (see below) were measured. Next, 100 μL of the first donor sample – either 5% theophylline (TH) or 2% indomethacin (IND) suspensions in 60% propylene glycol – was applied to the membrane. This setup ensured sink conditions for the selected drugs. Samples of the acceptor phase (300 μL) were withdrawn every 2 h over 10 h and were replaced with the same volume of PBS. During this period, a steady state situation was reached (see the permeation profiles in Figs. S1 and S2, Supplementary material). After the first 10 h-long permeation experiment, the applied donor suspension was carefully washed with PBS, pH 7.4, and the residual PBS was removed using cellulose swabs. The membranes were allowed to equilibrate for 12 h. Afterward, 100 μL of the second donor sample (TH or IND) was applied. The permeation experiment was repeated as described above. To verify that the first experiment did not alter the outcome from the second one, we changed their order in some membranes. The permeation profiles did not differ. Thus, this setup was used to obtain more data from each membrane. For further validation and comments, see our previous work [29].

2.9. Measurements of relative water loss through the membranes

The relative water loss through the model membranes was measured using equipment for transepidermal water loss measurement (TEWL) [g/h/m^2]: the Tewameter® TM 300 probe and Multi Probe Adapter Cutometer® MPA 580 (CK electronic GmbH, Köln, Germany) were used. The physical basis of the measurement is the diffusion principle in an open chamber. The water vapor pressure gradient is indirectly measured by two pairs of sensors (temperature and relative humidity), which are located at two different heights inside a hollow cylinder (height of 2 cm, diameter of 1 cm). The probe head is placed horizontally on the measured surface at a constant pressure, and its small size minimizes the influence of air turbulence inside the probe [30]. To measure the water loss through the model membranes, the upper part of the Franz-type diffusion cell was removed and the probe was placed on the membrane holder containing a cylindrical hole with a diameter of 0.8 cm (0.5 cm^2), 0.6 cm from the membrane surface.

The measuring time was usually between 80 and 100 s, and the average steady-state value was recorded. The environmental conditions were comparable during all measurements: ambient air temperature of 26–29 °C and relative air humidity of 40–46%. Because the usage of the membrane holder affects the measured values, the obtained data were relative and were normalized according to the equation: TEWL normalized = TEWL / (average TEWL of the control samples).

2.10. Measurements of the electrical impedance

After the relative water loss measurements, the electrical impedance [kΩ] was measured using an LCR meter 4080 (Conrad Electronic, Hirschau, Germany; measuring range of 20 Ω to 10 MΩ, error at kΩ values <0.5%), which was operated in a parallel mode with an alternating frequency of 120 Hz. The electrical impedance is commonly used to non-invasively and rapidly evaluate skin integrity. An equivalent model of skin impedance is a circuit composed of a resistor and capacitor in parallel [31]. The impedance opposes the alternating current and includes resistance but also accounts for capacitance [32]. The direct current resistance of the skin is a product of the resistivity and the thickness of the stratum corneum. The resistivity of the skin is inversely proportional to the permeability to ions or polar chemicals. A good estimate of skin resistance is the electrical impedance measured in parallel mode at a frequency of 100 Hz [33]. We used a similar setting of the LCR meter to characterize the model lipid membranes. The obtained values represent a measure of the opposition to alternating current. We added 500 μL of PBS, pH 7.4, in the donor compartment of each Franz-type diffusion cell. The impedance of the lipid membranes was obtained by immersing the tip of stainless steel probes into PBS in the donor and acceptor compartments (one probe per compartment) of the Franz-type diffusion cell. The measurements were taken for each cell before the application of the donor samples. Then, the PBS was carefully removed from the donor compartment.

2.11. High performance liquid chromatography (HPLC) of model permeants

The TH- and IND-containing samples were measured by isocratic reverse-phase HPLC using a Shimadzu Prominence instrument (Shimadzu, Kyoto, Japan) consisting of LC-20AD pumps with a DGU-20A3 degasser, SIL-20A HT autosampler, CTO-20AC column oven, SPD-M20A diode array detector, and CBM-20A communication module. Data were analyzed using the LCsolutions 1.22 software. Reverse phase separation of TH was achieved on a LiChroCART 250-4 column (LiChrospher 100 RP-18, 5 μm, Merck, Darmstadt, Germany) at 35 °C using 4:6 methanol/0.1 M NaH_2PO_4 (v/v) as a mobile phase at a flow rate of 1.2 mL/min. Acceptor phase sample (20 μL) was injected into the column, and the UV absorption of the effluent was measured at 272 nm, with a bandwidth of 4 nm. The retention time of TH was 3.2 ± 0.1 min. The IND samples were assayed on a LiChroCART 250-4 column (LiChrospher 100 RP-18, 5 μm, Merck) using a mobile phase containing 90:60:5 acetonitrile/water/acetic acid (v/v/v) at a flow rate of 2 mL/min. Next, 100 μL of acceptor phase sample was injected into the column, which was maintained at 40 °C. The UV absorption was monitored at a wavelength of 260 nm, the bandwidth was 4 nm, and the retention time of IND was 3.1 ± 0.1 min. Both methods were previously validated [22].

2.12. Permeation data evaluation

Using the measured concentrations of TH and IND and the Franz-type diffusion cell's volumes, the cumulative amounts of TH and IND that penetrated across the lipid membrane were calculated. The cumulative amounts were corrected for the acceptor phase replacement. For example, the cumulative amount at the time t = 6 h was calculated according to the following equation: $m_{6\,h} = (c_{6\,h} \times V + c_{4\,h} \times 0.3 + c_{2\,h} \times 0.3) / A$, where $m_{i\,h}$ is the cumulative amount at a time *i* h, $c_{i\,h}$ is the concentration [mg/mL] at the time *i* h, V is the acceptor phase volume in mL, and A [cm^2] is the diffusion area. The cumulative amounts were plotted against time, and the steady state flux of TH or IND [μg/cm^2/h] was calculated as a slope of the linear regression function obtained by fitting the linear region of the plot in Excel (see Figs. S1 and S2, Supplementary material). The data are presented as the means ± SEM, and the number of replicates is given in the pertinent figure. One-way analysis of variance with Dunnett's post hoc test method was used for the statistical analysis of the effect of SM.

2.13. X-ray powder diffraction

The lipid mixtures for the X-ray powder diffraction (XRPD) measurements were prepared in the same way as those for permeation experiment, but the lipids were sprayed onto a 22 × 22 mm supporting cover glass instead of the supporting filters. Prior to the measurement, the samples were heated to 90 °C, equilibrated at this temperature for 10 min and allowed to cool down for approximately 3 h. The XRPD data were collected at ambient temperature with an X'Pert PRO θ–θ powder diffractometer (PANalytical B.V., Almelo, Netherlands) with parafocusing Bragg–Brentano geometry using CuK_α radiation (λ = 1.5418 Å, U = 40 kV, I = 30 mA) in modified sample holders over the angular range of 0.6–30° (2θ). Data were scanned with an ultrafast detector X'Celerator with a step size of 0.0167° (2θ) and a counting time of 20.32 s $step^{-1}$. The data were evaluated using the software package HighScore Plus (PANalytical B.V., Almelo, Netherlands). The XRPD diffractograms show the scattered intensity as a function of the scattering vector Q [nm^{-1}], which is proportional to the scattering angle θ according to the equation: $Q = 4\pi \sin\theta/\lambda$ (λ = 0.15418 nm is a wavelength of the X-rays). The repeat distance *d* [nm] characterizes the regular spacing of parallel lipid bilayers arranged on a one-dimensional lattice. This lipid arrangement is called a lamellar phase (*L*). The diffractograms of lamellar phases exhibit a set of Bragg reflections whose reciprocal spacings are in characteristic ratios of $Qn = 2\pi n/d$ (reflection's order number $n = 1, 2, 3\ldots$). The repeat distance *d* was obtained from the slope *a* of a linear regression function of the dependence $Qn = a.n$, according to the equation $d = 2\pi/a$.

3. Results

3.1. Permeability of the model membranes containing a single type of Cer (SM/CerNS/Chol/FFA/CholS)

First, we prepared a simple model of the SC lipid barrier containing a single type of Cer: CerNS/Chol/FFA/CholS. The chosen lipid ratio correlates with the lipid composition of human SC [28,34]. To study how SM affects the membrane barrier function, we replaced 25%–100% of CerNS by SM, which simulates an accumulation of SM at the expense of Cer and mimics the aSMase deficiency in the SC. We used SM from bovine milk (bmSM) for the preliminary permeation experiments because it predominantly contains long acyl chains (according to the supplier: 16% C16:0, 20% C22:0, 34% C23:0, 21% C24:0, 3% C24:1 and 6% unknown chains) similarly to CerNS (C24:0). In an attempt to verify these results on a slightly different model, the experiments were partly repeated with chicken egg SM (eSM) that mainly contains 16-carbon acyl chains (86% C16:0). However, we did not find any differences between the permeability of these eSM- and bmSM-containing membranes (not shown). Therefore, these results are presented together in Fig. 2A–C.

We investigated these membranes by using four permeability markers: 1) flux of theophylline [μg/cm^2/h] (TH, M = 180.164 g/mol, log P ~ 0); 2) flux of indomethacin [μg/cm^2/h] (IND, M = 357.787 g/mol, log P ~ 4.3); 3) electrical impedance [kΩ × cm^2]; and 4) relative water loss [a.u.]. TH and IND represent model drugs with different molecular sizes, lipophilicities and mechanisms of permeation through the lipid membrane. In general, small hydrophilic molecules, such as TH, diffuse through density fluctuations in the lipid chains that open up free volume

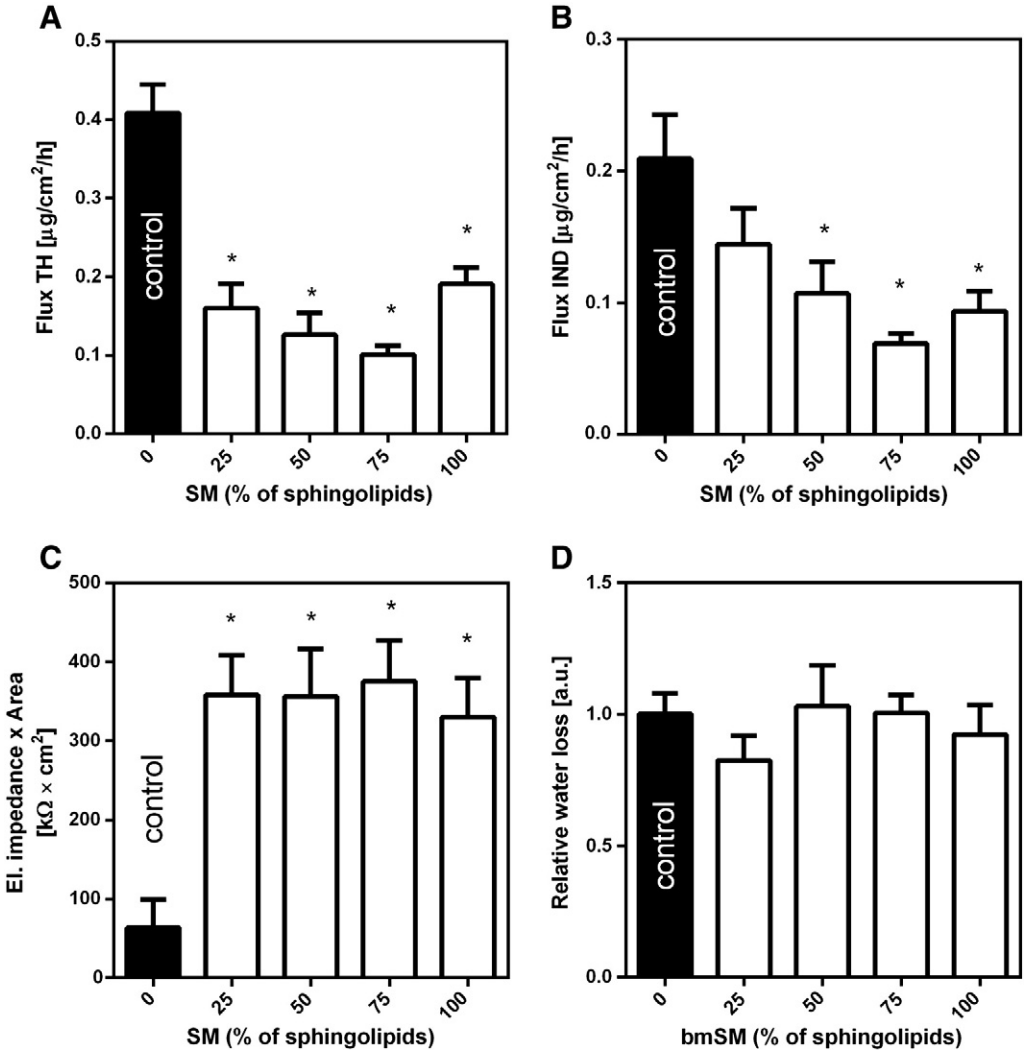

Fig. 2. Permeability of SM/CerNS/Chol/FFA/CholS membranes: (A) Flux of theophylline (TH); (B) flux of indomethacin (IND); (C) electrical impedance × area of membrane; (D) relative water loss. Data are presented as the means ± standard error of mean (SEM), $n = 5–26$. * statistically significant against control ($p < 0.05$).

pockets. Large lipophilic molecules, such as IND, will likely permeate through the membrane due to lateral diffusion along SC lipid bilayers [35]. The flux of TH through the membrane with no SM reached a value of 0.41 ± 0.04 μg/h/cm^2 (flux ± standard error of mean, SEM), which is comparable to the permeability of the previously used model CerNS/Chol/lignoceric acid/CholS that showed a TH flux of 0.36 ± 0.04 μg/cm^2/h [29]. The gradual replacement of CerNS by SM in the range from 25% to 100% SM decreased the permeability to TH (TH flux was in the range of 0.10 ± 0.04–0.19 ± 0.02 μg/cm^2/h, Fig. 2A). Similar results were obtained with IND. The flux of IND through the membranes without SM was 0.21 ± 0.03 μg/cm^2/h and was lower than value reached with the CerNS/Chol/lignoceric acid/CholS model (0.32 ± 0.08 μg/cm^2/h) [29]. When CerNS was replaced by SM, the permeability to IND decreased (IND flux values were in the range of 0.07 ± 0.01–0.14 ± 0.03 μg/cm^2/h, Fig. 2B). The pertinent permeation profiles are given in the Supplementary material (Figs. S1 and S2).

We used an LCR meter to characterize the model lipid membranes by measuring their electrical impedance, which express the opposition to an alternating current. The electrical impedance of the control membrane with no SM was 64 ± 35 kΩ × cm^2, which represents a relatively low value. These measurements were also highly variable. For a comparison, the electrical impedance of a previously used model with only one FFA (CerNS/Chol/lignoceric acid/CholS) was 334 ± 43 kΩ × cm^2 [29]. The more heterogeneous free fatty acid composition in this work, in particular the presence of short FFA, most likely contributed to the lower electrical impedance in comparison with the previously studied lipid membranes with only lignoceric acid. After the partial or total replacement of CerNS by SM, a significant increase in electrical impedance was observed: the membranes containing SM reached values from 330 ± 50 kΩ × cm^2 to 376 ± 52 kΩ × cm^2 (Fig. 2C).

The fourth permeability marker of the model membranes was the relative water loss (Fig. 2D). The equipment for transepidermal water loss (TEWL) is mostly used for *in vivo* measurements in patients with the aim of evaluating the condition of the skin barrier [36]. In principle, it is also possible to measure water loss *in vitro* [37–40]; thus, we utilized this method to estimate the water loss through our artificial bmSM/CerNS/Chol/FFA/CholS lipid membranes. The relative water loss of the control membranes was normalized to 1.00 ± 0.19 a.u. The membranes containing bmSM lost water in the range of 0.82 ± 0.09 and 1.03 ± 0.16 a.u., and the changes were not significant relative to the control.

The above-mentioned results indicate that, in the case of a simple model based on a single CerNS, SM actually improves the barrier properties against small hydrophilic molecules (TH), larger hydrophobic molecules (IND) and alternating current. No significant effect was detected in the case of the water permeation barrier. These results are

contradictory in the context of *in vivo* experiment findings on the animal model [16]. We hypothesized that these surprising results could be caused by the simplicity of the model containing only one type of ceramide — CerNS. Thus, we prepared model membranes that more closely mimicked the SC lipid barrier.

3.2. Permeability of model membranes based on isolated human SC Cer (bmSM/hCer/Chol/FFA/CholS)

We isolated the human Cer fraction of the stratum corneum (hCer). HPTLC analysis confirmed that the isolated Cer fraction contained Cer in similar proportions to those of the human SC, including the very long acyl Cer of the EO classes. We found the following composition of human SC Cer fraction in wt.% (2 analyses of the hCer sample pooled from 6 subjects): CerEOS 3.3–4.7%; CerNS 9.9–10.4%; CerEOP 1.2–3.4%; CerNP + CerEOH 46.2–46.6%; CerAS + CerNH 21.3–27.9%; CerAP 5.0–6.2%; and CerAH 4.8–9.0%. The average human SC Cer molecular weight of 692.4 g/mol was calculated using the data on the Cer composition and average alkyl chain length [41]. The membrane composition was maintained at the same ratio of sphingolipids/FFA/Chol/CholS. We used hCer instead of CerNS, and the hCer were subsequently replaced by increasing fractions of bmSM (25%–100%). The permeability of these membranes was evaluated in the Franz-type diffusion cells (Fig. 3A–D). The permeability markers were identical with those used in the simpler bmSM/CerNS/Chol/FFA/CholS membranes. The permeability of the control sample with no SM for TH was 0.40 ± 0.05 μg/cm^2/h, which is similar to the model based on CerNS (Fig. 3A). This result is surprising given the presence of the acylCer in the hCer model. Nevertheless, the differences between these two models manifested in the presence of 25% and 50% bmSM. When the 25 and 50% of hCer was replaced by bmSM, the permeability of these membranes increased to 0.71 ± 0.05 and 0.57 ± 0.05 μg/cm^2/h, respectively. The replacement of 75% of hCer by SM led to a decrease in the membrane permeability to TH (flux of 0.24 ± 0.02 μg/cm^2/h) compared to that with lower SM model. When bmSM replaced all the hCer, the permeability to TH was also lower (0.24 ± 0.03 μg/cm^2/h) than that of the control membrane.

The IND flux through the control sample (0.23 ± 0.02 μg/cm^2/h) was also similar to that of the model containing only CerNS (Fig. 3B). The permeability to IND slightly and non-significantly increased to 0.27 ± 0.03 and 0.28 ± 0.04 μg/cm^2/h in the membranes with 25% and 50% SM, respectively. Further replacement of hCer by SM caused a significant decrease in the permeability to IND, showing flux values of 0.11 ± 0.01 μg/cm^2/h and 0.08 ± 0.01 μg/cm^2/h in the 75% and 100% SM membranes, respectively.

The electrical impedance showed a similar biphasic dependence on the bmSM/hCer ratio (Fig. 3C). The electrical impedance of the control membranes mimicking a healthy SC lipid barrier was 263 ± 19 kΩ × cm^2,

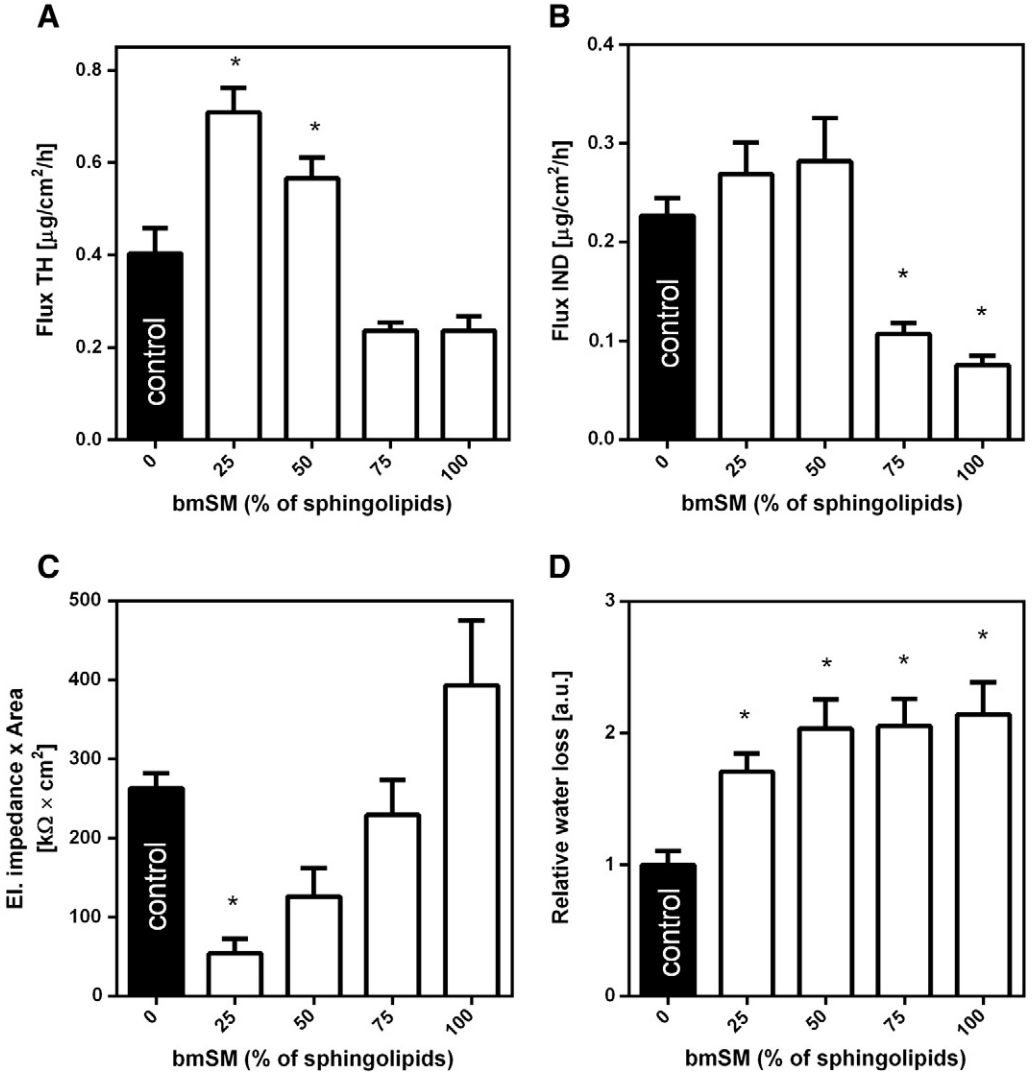

Fig. 3. Permeability markers of bmSM/hCer/Chol/FFA/CholS membranes. (A) Flux of theophylline (TH); (B) flux of indomethacin (IND); (C) electrical impedance × area of membrane; (D) relative water loss. Data are presented as the means ± standard error of the mean (SEM), $n = 6$–13. * statistically significant against control ($p < 0.05$).

which indicates a good barrier to alternating current in comparison with the barrier provided by the CerNS/Chol/FFA/CholS membranes. The electrical impedance decreased in the membranes where 25% and 50% hCer were replaced by bmSM (54 ± 19 kΩ × cm^2 and 126 ± 36 kΩ × cm^2, respectively). In contrast, the further increase in the bmSM/hCer ratio normalized the electrical impedance in comparison to that of the control, and the full substitution of hCer by SM even improved the barrier properties of that membrane to alternating current compared with the control.

The relative water loss through the membrane was most influenced by the increased SM/hCer ratio and proved to be a key parameter for understanding the effect of SM on the membrane barrier properties (Fig. 3D). The water loss of the control hCer/Chol/FFA/CholS was mathematically normalized to 1.00 ± 0.11 a.u. All membranes containing bmSM showed higher water loss than that of the control with water loss values between 1.71 ± 0.14 a.u. and 2.1 ± 0.2 a.u. Thus, the water loss through the membrane was the only permeability marker that indicated a barrier-impairing effect of SM in the whole studied range of the SM/hCer molar ratios. The described effect on the water permeability barrier was only observed in the model containing hCer, not in the simple membranes containing only one Cer class.

3.3. Microstructure of CerNS-based membranes (bmSM/CerNS/Chol/FFA/CholS)

To understand the mechanism underlying the observed differences in permeability, X-ray powder diffraction (XRPD) data were collected on the lipid membranes that were applied to a supporting cover glass. The diffractograms of the bmSM/CerNS/Chol/FFA/CholS mixture are shown in Fig. 4. All the diffractograms contained two reflections of crystalline cholesterol at Q ~ 1.85 and 3.68 nm^{-1}, corresponding to the first and second order reflections, respectively. The repeat distance d was estimated from the slope of the center of reflection in Q vs the order of the reflection n giving d = 3.4 nm. This repeat distance characterizes stacked cholesterol bilayers and is in agreement with the reported data [42]. Crystalline Chol has been found also in the human SC [43], model SC membranes with isolated pig Cer/Chol/FFA [7,25] and SC models with synthetic Cer [29,44].

The diffractogram of the control sample without SM (Fig. 4) also contained another series of peaks at Q = 1.19, 2.37, 3.55, 4.72 nm^{-1}, giving the repeat distance d = 5.32 nm. These peaks were attributed to the lamellar phase *La* that is analogous to the so-called short periodicity phase (SPP) that occurs in the SC and is, in fact, longer (6.4 nm) [43].

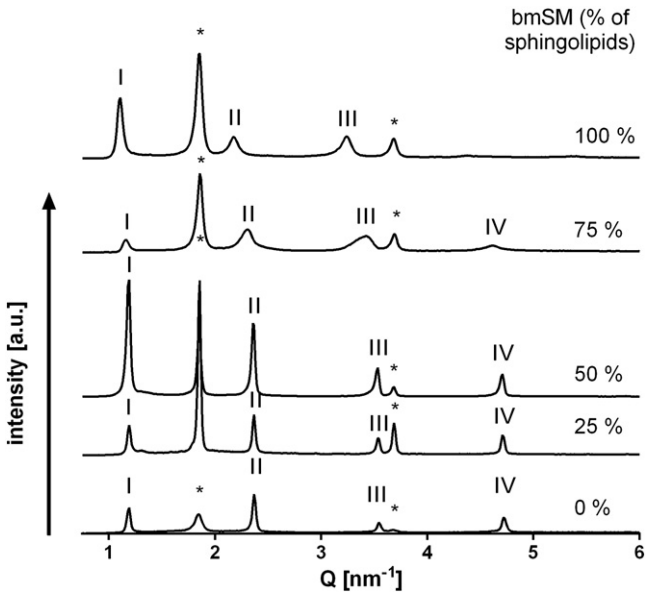

Fig. 4. XRPD diffractograms of bmSM/CerNS/Chol/FFA/CholS model membranes. Roman numerals mark the *La* phase (short periodicity phase, SPP); asterisks mark the crystalline cholesterol (Chol).

The sample containing 25% bmSM instead of CerNS (Fig. 4) expressed reflections of crystalline Chol (d = 3.4 nm) and the lamellar phase *La* (d = 5.34 nm). At 50% bmSM, we found d_{La} = 5.35 nm. Samples with 75% and 100% bmSM also showed two regularly arranged phases — crystalline Chol and the lamellar phase *La* with d_{La} = 5.45 nm and d_{La} = 5.8 nm, respectively.

The dependence of d_{La} on the bmSM content is shown in Fig. 5A. The lamellar thickness increased nonlinearly as the bmSM fraction increased. The repeat distance d_{La} increased from 5.32 nm in the membrane without bmSM to 5.8 nm when all the CerNS molecules were replaced with bmSM. The ratio of the full width at half maximum of the 2nd (Δ s2) and 1st order (Δ s1) reflections is often used to compare the extent of bilayer fluctuations [45]. The ratio Δ s2/Δ s1 of the *La* phases at increasing bmSM fraction is depicted in Fig. 5B. The highest ratio Δ s2/Δ s1 > 2 was observed in membranes with 75% and 100% bmSM and indicated a higher rate of fluctuations and a less ordered lamellar arrangement than in the membranes with lower bmSM content. Δ s2/Δ s1 ratio values greater than 2 are typically reported for phospholipid bilayers [45]. Obviously, the behavior of membranes with high bmSM content resembled that of more hydrated and fluctuating phospholipid bilayers. In the context of the permeation experiment, it is surprising that the membrane permeability remains low despite the less ordered and fluctuating arrangement of membranes with high bmSM content.

3.4. Microstructure of membranes containing eSM and Cer NS (eSM/CerNS/Chol/FFA/CholS)

To investigate the influence of SM with a different chain length distribution, XRPD experiments were performed in the samples containing eSM/CerNS/Chol/FFA/CholS. The corresponding diffractograms are shown in Fig. S3A, Supplementary material. All the diffractograms contain first and second order reflections of crystalline cholesterol with d = 3.4 nm. We identified also *La* lamellar phases. The repeat distances d are plotted against the eSM fraction in Fig. S3B, Supplementary material. The control without eSM (CerNS/Chol/FFA/CholS) was measured in the previous series, and we found d_{La} = 5.32 nm. When CerNS was partially replaced by eSM, the d_{La} slightly increased to 5.38 nm at 50% eSM. Further replacement of CerNS caused an abrupt increase in the repeat distance to 5.57 nm at 75% eSM and 5.79 nm at 100% eSM; this increase is similar to the membranes with bmSM. The obtained structural data of the eSM/CerNS/Chol/FFA/CholS membranes are analogous to those containing bmSM. Surprisingly, both lipid mixtures, either with bmSM or eSM, maintained very similar d_{La} values in the whole range of SM/CerNS ratios, despite the different acyl chain length distributions of bmSM and eSM.

3.5. Microstructure of hCer-based membranes (bmSM/hCer/Chol/FFA/CholS)

Before the XRPD measurement, the membranes containing an hCer fraction instead of CerNS were treated in the same manner as those with bmSM/CerNS/Chol/FFA/CholS. The diffractograms are shown in Fig. 6. The crystalline Chol fraction with a repeat distance d = 3.4 nm is present in all the prepared lipid mixtures.

The mixture containing 0% bmSM (hCer/Chol/FFA/CholS) expressed three additional lamellar phases, which were identified using a linear least square fitting of the plot of the center of reflection in Q vs the reflection order n. The lamellar phases *La* and *Lb* with the short repeat distances showed reflections at Q = 1.16, 2.28, 3.4, 4.52 nm^{-1} and Q = 1.60, 3.22 nm^{-1}, respectively. Their estimated repeat distances were d_{La} = 5.56 nm and d_{Lb} = 3.96 nm. The repeat distance d_{La} = 5.56 nm

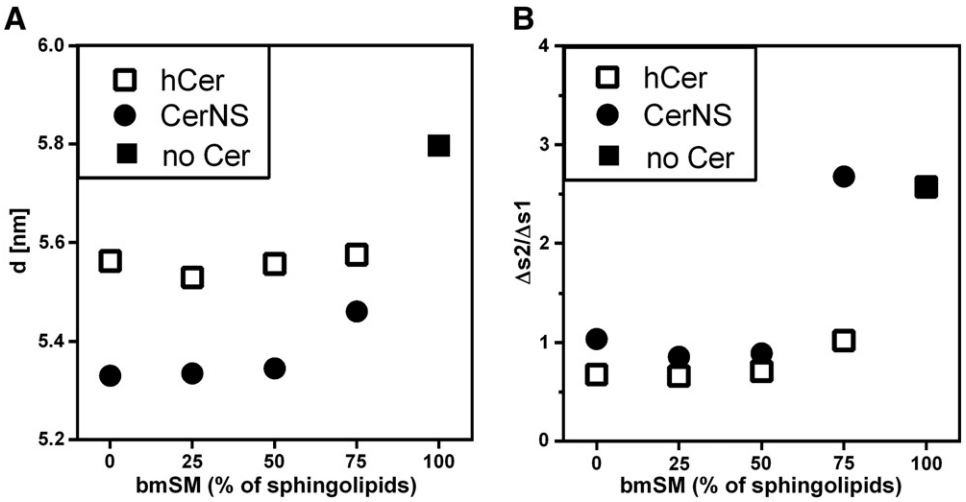

Fig. 5. Repeat distances of the *La* lamellar phase (SPP) as a function of bmSM:Cer ratio (A). The ratio of the full width of half maximum of the 2nd (Δ s2) and 1st order (Δ s1) *La* phase reflections as a function of bmSM:Cer ratio (B). The filled square marks bmSM/Chol/FFA/CholS.

was slightly higher than the corresponding repeat distance observed in the CerNS/Chol/FFA/CholS sample (5.32 nm). The sample also contains another set of reflections at Q = 1.06, 1.50, 1.98, 2.94, 3.93 nm^{-1}, which were classified as orders $n = 2, 3, 4, 6, 8$. These reflections belong to the lamellar phase *Lc* of $d_{Lc} = 12.7$ nm. A similar phase called the long periodicity phase (LPP) with a repeat distance of 13.4 nm has been observed in the human SC [46] as well as in model lipid membranes with isolated porcine ceramides [8] ($d = 13$ nm) and [7] ($d = 12$–13 nm) or with synthetic ceramides [44] ($d = 11.6$ nm). The basic requirement for the formation of LPP are considered to be the acylCer of the EO classes, *e.g.*, Cer EOS, formerly known as Cer 1 [8,7].

When the 25% hCer was replaced with bmSM, the diffractogram showed a much simpler structure. We found the crystalline Chol phase and two lamellar phases: *La* with a repeat distance of $d_{La} = 5.53$ nm (Q = 1.17, 2.29, 3.42, 4.55 nm^{-1}) and *Lb* with $d_{Lb} = 4.21$ nm (Q = 1.50, 2.98 nm^{-1}). When increasing the bmSM fraction to 50%, d_{La} slightly shifted to a higher value (5.56 nm). The first order reflection of the *Lb* phase was at Q = 1.42 nm^{-1}, while the second order reflection

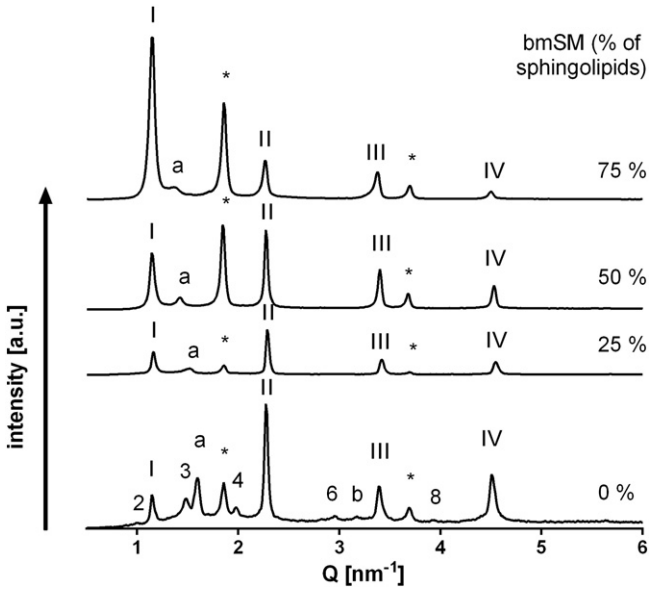

Fig. 6. XRPD diffractograms of bmSM/hCer/Chol/FFA/CholS. Roman numerals mark the *La* phase (short periodicity phase, SPP); Arabic numerals mark the *Lc* phase (long periodicity phase, LPP); asterisks mark crystalline cholesterol (Chol); and letters mark the additional lamellar phase *Lb*.

of the *Lb* phase disappeared. The calculated d_{Lb} was 4.53 nm. A similar structure was present at 75% bmSM: $d_{La} = 5.58$ nm and d_{Lb} (from the position of the 1st order maximum) = 4.77 nm. The structure of bmSM/Chol/FFA/CholS (100% bmSM) has been described above. The repeat distance of the *Lb* phase increased linearly ($R^2 = 0.998$) in the range from 0% to 75% bmSM (not shown). Moreover, the fluctuations of the lamellar arrangement occurred more frequently at high fractions of bmSM than in the membranes with less bmSM, and these fluctuations led to an increased Δ s2/Δ s1 ratio, especially at 100% bmSM (Fig. 5B). We compared the parameters of the *La* phase of the CerNS-based and hCer-based membranes in Fig. 5A. The lipid mixtures containing CerNS formed the *La* phase with a lower repeat distance than those containing hCer in the range from 0% to 75% bmSM. The repeat distances of both lipid mixtures (CerNS- based and hCer-based) non-linearly increased with increasing bmSM fraction.

3.6. Wide angle X-ray diffraction

The diffractograms of the bmSM/CerNS/Chol/FFA/CholS and bmSM/hCer/Chol/FFA/CholS membranes in the Q range of 14–18 nm^{-1} are depicted in Fig. 7. This wide angle region provides information about molecular packing (short range organization); in our case, we obtained information about the lateral arrangement of the lipid hydrocarbon chains. There were two peaks at Q ~ 15.1 nm^{-1} and 16.7 nm^{-1} in the control membranes without bmSM (both CerNS/Chol/FFA/CholS and hCer/Chol/FFA/CholS). Their corresponding repeat distances of 0.41 nm and 0.37 nm are typical of a tight orthorhombic chain packing [47]. The replacement of 25% of CerNS or hCer by bmSM did not qualitatively change the hydrophobic chain ordering because both reflections were still present. At all higher fractions of bmSM, we observed only one reflection at Q ~ 15.1 nm^{-1} in both SC models with a corresponding d ~ 0.41 nm. A single reflection at $d = 0.41$–0.42 nm has been reported to indicate less tight hexagonal chain packing [47]. The effect of bmSM on the hydrophobic chain packing depended on the bmSM/Cer ratio. If the bmSM/Cer ratio was low, the chains at least partially formed the orthorhombic phase. Higher fractions of bmSM led to hexagonal chain packing.

4. Discussion

The conversion of SM to Cer by SMases is an important process for maintaining the homeostasis of permeability in mammalian skin and seems to be particularly involved in early barrier recovery [48]. For example, the epidermal aSMase deficiency in Niemann–Pick patients

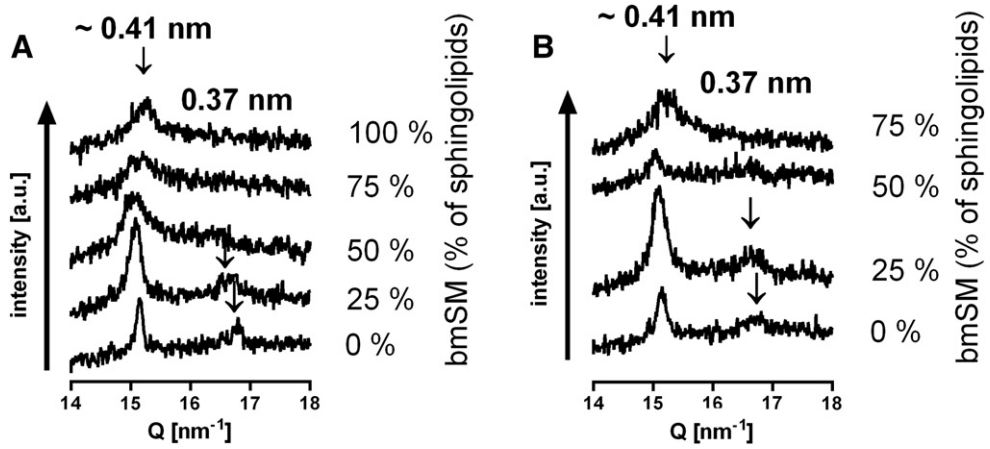

Fig. 7. Wide angle X-ray diffraction region of XRPD diffractograms of bmSM/CerNS/Chol/FFA/CholS (A) and bmSM/hCer/Chol/FFA/CholS (B); arrows indicate the positions of the reflections.

delays the barrier recovery after an acute insult, and the role of SM-to-Cer hydrolysis in this process was further confirmed by the administration of aSMase inhibitors to mice, which led to an increase in the SM content and a reduction in the normal SC lipid lamellae [16]. Decreased epidermal SMase (both acid and neutral) activity was also found in atopic dermatitis patients and was correlated with reduced Cer content and a disturbed barrier function [17]. The activity of this Cer-generating enzyme decreases also with aging [49,50].

In this work, we explored the biophysical properties underlying incomplete SM-to-Cer processing on a molecular level using lipid membrane models. These models are based on an equimolar mixture of Cer (either a single Cer, CerNS, or a full hCer fraction isolated from the human SC), FFA and Chol with 5 wt.% CholS mimicking the SC lipid composition [28,34]. To simulate decreased SMase activity, Cer was partly (by 25–75%) or fully substituted by SM. Although these percentages are likely higher than those encountered in the above mentioned skin disorders, we chose these ratios to study the biophysical consequences of SM-to-Cer conversion in a broader sense.

4.1. Effects of SM on the permeability of the model membranes

The first experiments were focused on how the SM/Cer ratio affects the permeability of the SC lipid membrane model. Our results from the simple model based on a single class of Cer were rather surprising: the replacement of CerNS by SM actually *improved* the permeability of the model lipid membranes as measured by the steady-state flux of TH, the steady-state flux of IND, and the electrical impedance, whereas the water permeability barrier remained essentially unchanged (Fig. 2). We hypothesized that these results, which are basically the opposite of the *in vivo* situation that we wanted to mimic, might have been caused by the lack of heterogeneity in the Cer of our first model.

Next, we prepared a model mimicking the SC lipid barrier more closely. We extracted the barrier lipids from the human SC and, to be able to control the Cer/SM ratio, we chromatographically separated the Cer fraction, termed hCer in this paper. In these hCer model membranes, the replacement of 25%–50% of Cer by SM indeed disturbed the barrier properties as indicated by the increase in the flux of TH and the decreased electrical impedance. When SM was the prevalent sphingolipid in the model membranes (that is, 75% and 100% of hCer was replaced by SM), it inversely improved their barrier properties compared to those of the control membranes (Fig. 3). This type of concentration-dependent biphasic effect was not detected in the case of the water permeability barrier: the water loss through the membranes was higher at all the studied SM/hCer molar ratios in comparison with the control without SM.

These results suggest that the importance of SM-to-Cer epidermal processing might be to control water loss from the body. The penetration of exogenous compounds, modeled here by the flux of TH and IND, seems to be relatively well suppressed by the more polar Cer precursor, SM. In fact, apart from its role in the skin, SM is known as a component of cellular membranes and has been found to be an important molecule in various cell signaling events. SM has a strong ability to stabilize the bilayer configuration [51]. SM and glycosphingolipids play an important role in reducing membrane permeability, and they require cholesterol to mediate this effect [52,53]. For example, low permeabilities of SM bilayers to water and glucose have been reported [53,54]. The biological functions of SM also include its role as a direct precursor of Cer, which in turn affects the membrane structure in many ways (*e.g.*, lipid scrambling, membrane permeability increase, pore formation and endocytosis) [55].

The decrease in permeability of our simple CerNS-based model with increased SM/Cer ratio is, in fact, in a good agreement with the SM/Cer behavior in other simple membrane systems. Both externally added or enzymatically produced Cer induce release of the contents of mixed SM/phospholipid-based unilamellar vesicles. Two properties of Cer, namely its capacity to induce negative membrane curvature and its tendency to segregate into Cer-rich domains, appear to be important in the membrane restructuring process [56]. This explanation is in agreement with the low permeability of our SM/Chol/FFA/CholS model. However, the reported properties of vesicles composed of mixed lipid species cannot be simply transferred to a highly-ordered multilamellar system such as the SC model membranes. Nevertheless, we can say that SM does not *per se* increase the permeability of either the vesicles or the SC lipid models to relatively small molecules. Only the water permeability barrier is apparently weakened by the replacement of hCer by SM in our SC lipid model.

4.2. Microstructure of model membranes in the small angle X-ray diffraction region

To elucidate the behavior of SM in our SC lipid models, we studied the membranes by XRPD. Both the single CerNS model and the hCer-based one formed the short periodicity phase *La*; however, the repeat distance of *La* was larger in the hCer model than in CerNS (Fig. 5A). This increased repeat distance is most likely caused by an increase in the lipid bilayer thickness, which also depends on the average chain length of the lipids. While CerNS has a defined chain length of C24 and 42 total carbons, the hCer fraction represents a heterogeneous group with a complex acyl chain length distribution, with the most abundant Cer in human SC containing between 40 and 52 carbons

[41]. The average chain length of hCer is higher compared to that of CerNS and can be considered a reason for the increased repeat distance of *La*. However, a similar exchange between bmSM and eSM with a different average acyl chain length, as discussed below, did not show a similar effect on the repeat distance of the corresponding membranes. This difference could be connected to a specific organization of the membrane containing hCer. The permeability to TH and IND of the controls differed neither for the CerNS-containing membranes nor for hCer-containing ones, and the small difference in their repeat distances does not seem to play a role.

Increases in the SM/Cer ratio increase the repeat distance of *La* with the most significant changes at 75% and 100% replacement of Cer by SM (Fig. 5A). Furthermore, SM at high fractions significantly disorders the lamellar arrangement of the lipid membranes (Fig. 5B). The disordering effect is less pronounced in the case of the hCer-based model. The acyl chain length distribution of bmSM (mostly from 22 to 24 carbons) is comparable to that of CerNS, *i.e.*, C24, and most likely does not explain the increased repeat distance. In contrast to Cer, SM has a larger and more hydrated polar head group. The bovine brain SM can trap more water molecules [57,58] than CerNS can [59–61]. The repeat distance of the lamellar phase created by bovine brain SM can vary with the hydration level in the range of 6.35–7.49 nm at 25 °C [57] and with osmotic stress in the range of 6.34–7.56 nm at 20 °C [62]. *N*-tetracosanoyl SM with a defined acyl chain length attained a repeat distance that was modulated by osmotic stress between 6.38 and 7.43 nm [62], which is very similar to that of bovine brain SM. The dominant acyl species of bovine brain SM are C18:0 (45%) and C24:1 (27%) [57]. These findings indicate that SM can provide more hydration than Cer and, as a consequence, its lamellar repeat distance is variable. The larger polar head group of SM most likely caused the increase in the *La* repeat distance with increasing SM content in our model *via* increasing the polar region of the lipid lamellae. Because we did not maintain a defined hydration level in our sample, we also cannot exclude its possible effect on the SM-containing membranes.

Interestingly, very similar behavior was found when the eSM with shorter acyl chains was used instead of bmSM. The structural data of eSM/CerNS/Chol/FFA/CholS (Fig. S3 in Supplementary material) are included here for comparative purposes. The repeat distances of the lamellar phases *La* are almost identical in the membranes containing bmSM or eSM in the same percentage. Molecules of bmSM are characterized by an inherently asymmetric nature because of the length mismatch between the sphingoid base (18 carbons) and the usually long *N*-linked acyl chain [55]. Therefore, the bmSM forms a tilted and partially interdigitated gel phase [63]. The acyl chains of eSM (86% of the chains are C16:0) are shorter than those of bmSM as well as those of CerNS and match with the sphingoid chains. Considering only the length of the hydrophobic chains, one would expect a longer repeat distance for bmSM-containing membranes in comparison with that of the membrane containing eSM. Such behavior has been described in phospholipids: the bilayer thickness, which is the main component of the repeat distance, increases with increasing chain length and saturation [64]. In addition, the presence of hCer with a longer average chain length increases the repeat distance of the *La* phase in comparison with that of membranes containing CerNS only. However, eSM did not decrease the repeat distance compared to that of bmSM in our model systems. To explain this finding, we must also consider the effect of Chol, which can either increase or decrease the width of the bilayer depending on the physical state and the chain length of the lipid before the introduction of Chol. Chol reduces the extent of methylene chain interdigitation [65] and disorders the hydrophobic chains near the center of the bilayer [62]. When equimolar Chol was added to the bovine brain SM, the repeat distance decreased and attained a narrower range of 5.93–6.63 nm in comparison to the range of the lamellae of pure bovine brain SM. The equimolar mixture SM with C24 acyl chain/Chol formed a lamellar structure with a repeat distance of 6.63–6.81 nm, slightly higher than that of the bovine brain SM/Chol mixture [58]. We suppose that the repeat distance of our membranes containing either bmSM or eSM is strongly modulated by Chol. In the membranes with eSM containing mostly 16C acyl, Chol may increase the width of the lamellae by removing the chain tilt of the gel-state lipids similarly to phospholipid bilayers. The repeat distance of the membrane with bmSM decreased upon the addition of Chol because the long chains must deform or kink to accommodate the significantly shorter cholesterol molecule [65]. Thus, we assume that Chol can compensate for the differences between the acyl chain lengths of eMS and bmSM. However, we have not observed this effect in the case of the hCer/CerNS exchange in the membranes with an analogous composition.

4.3. Lateral lipid organization of the model membranes

For the lateral lipid organization, the control membranes, either with CerNS or hCer, display orthorhombic chain packing similar to that found in healthy human skin [66]. This tight chain packing has been regarded as an indicator of good barrier function [67]. In our model membranes, the orthorhombic lattice persists when 25% of Cer is replaced by SM, but higher SM/Cer ratios (starting at 50% SM) change the short range organization of the lipid molecules from orthorhombic to hexagonal. However, this structural change does not correlate with the membrane permeability properties, *i.e.*, no abrupt increase in permeability was found at 50% SM when the orthorhombic packing dissolves. This result is in agreement with a recently published work showing that tight orthorhombic packing of molecules is not crucial for competent barrier function in an SC lipid model [68].

Saturated hydrophobic chains of SM have been reported to create a highly ordered phase [55] and to have a relatively high chain melting temperature [63]. SM usually undergoes a hydrocarbon phase transition as the temperature is increased through 35 °C [51,62]. This transition disappears in the presence of equimolar Chol [51,55]. The highly ordered chains preferentially interact with Chol, which helps to keep the chains in a liquid-ordered state [55,69]. Chol thus guarantees that the mostly saturated acyl chains of SM do not form excessively ordered gel phases in the membranes. The addition of equimolar Chol to either bovine brain SM or SM with C24 acyl changes the packing of the ordered hydrophobic chains to disordered chain packing to form a liquid-crystalline phase [62]. From this point of view, it is surprising that we observed a tight orthorhombic arrangement of hydrophobic chains at 25% bmSM and an ordered hexagonal arrangement at 50%–100% bmSM because in both cases, the membrane is saturated with Chol at ambient temperature. This propensity to form ordered membranes might be related to the third major component of the SC lipids, the very long saturated FFA molecules, which are also required for homeostasis of the epidermal barrier [70]. FFA containing 12 or more carbon atoms increase the main lipid phase transition of a dipalmitoylphosphatidylcholine–water model membrane [71]. Thus, protonated (uncharged) FFA lead to a rather tight lateral packing in the mixed membrane and a moderate ordering and hence stretching of the lipid chains [72]. This behavior of FFA may explain the relatively high order of our model membranes.

4.4. Long periodicity lamellar phase

The most important structural feature that differentiates the studied membranes and may explain the Cer-dependent effects of SM on the water barrier properties is the presence of the long periodicity phase (LPP, $d_{Lc} = 12.7$ nm) in the hCer/Chol/FFA/CholS membranes. LPP is considered to play an important role in skin barrier function, and long acylCer of the EO class (*e.g.*, EOS) are required for its formation [7]. Thus, it is not surprising that LPP is missing in the membranes containing only CerNS. Nevertheless, the molecular organization of the SC lipid lamellae remains unresolved. One approach emphasizes the importance of a fully extended Cer conformation as a key structure unit of the SC lamellae, where Chol is associated with a Cer sphingoid moiety and FFA is

associated with an acyl chain. However, this model does not specifically address the location of the long acylCer [73,74]. Other authors present a model of LPP containing Cer as well as long acylCer in the hairpin conformation with both chains pointing in the same direction [9]. McIntosh obtained the electron density profiles of LPP of hydrated model lipid membranes, which contained isolated porcine Cer [75]. His model proposed an asymmetric distribution of cholesterol and unsaturated linoleic chains of acylCer so that these two components avoid their mutual contact. Despite an extensive research effort, it is not clear whether LPP requires the extended conformation of Cer. Our results have shown that even a partial replacement of hCer with bmSM diminishes LPP formation. This result may be connected with the larger polar head group of SM and its higher water-binding properties that make the formation of the extended conformation unfavorable. Indeed, SM and cerebrosides pack in a typical bilayer arrangement with a parallel stacking of the hydrophobic chains [76,77], whereas Cer is more likely than bmSM to be able to form a fully extended conformation. We hypothesize that these properties of SM could contribute to the inhibition of LPP formation in bmSM/hCer/Chol/FFA/CholS membranes.

5. Conclusions

We showed how an altered SM/Cer ratio in model lipid membranes that mimic the skin barrier influences their permeability and structural parameters. In the CerNS-based model, the presence of SM actually *improves* the barrier properties against TH, IND and alternating electric current independently for the following factors: 1. the lamellar repeat distance; 2. presence of the orthorhombic chain packing; and 3. rate of ordering of the lamellar phase *La*. SM did not change the water loss through the membrane. These results show the limitations of such a simple membrane model containing only one type of Cer (CerNS), when another membrane compound is admixed (*e.g.*, SM). Thus, although such simple membranes may be reasonably good models for certain studies of basic lipid behavior, they must be used cautiously or replaced by a more relevant membrane system when mimicking a biological situation where lipid heterogeneity plays a role.

In the case of the hCer-based model, the effect of SM depends on the SM/Cer ratio. Low SM levels (up to SM/Cer molar ratio of 50:50) disturb the barrier properties of the membranes, whereas a higher SM content tends to decrease their permeability to chemicals (TH, IND) and their ability to conduct alternating current. This concentration-dependent effect does not correlate with the XRPD structural features of the model membranes (similarly to the CerNS-based model). This behavior most likely reflects the complexity of the drug permeation process and shows that this process is not fully understood.

An exception to this behavior is the water loss through the membrane. While the hCer/Chol/FFA/CholS membranes comprising LPP created a good barrier to water, the membranes with increasing proportions of SM controlled the water loss less efficiently. These results suggest that the importance of the natural release of Cer from SM is preventing desiccation. In agreement with this proposal, only the water loss through the hCer-based membranes correlates with their periodic lamellar structure. Thus, the presence of LPP plays a key role in homeostasis of the water barrier. Our results suggest that SM impairs the water permeability barrier via interfering with LPP formation in the studied range of SM fractions. This explanation agrees well with the *in vivo* findings from patients with Niemann–Pick disease [16] and atopic dermatitis [17], in which decreased aSMase activity was accompanied by impaired barrier function, which was diagnosed using transepidermal water loss (TEWL) measurements [16].

Acknowledgements

The publication is co-financed by the European Social Fund and the state budget of the Czech Republic, project no. CZ.1.07/2.3.00/30.0061, by Czech Science Foundation (13-23891S), and Charles University in Prague (SVV 260 062).

Appendix A. Supplementary data

Supplementary data to this article can be found online at http://dx.doi.org/10.1016/j.bbamem.2014.05.001.

References

[1] P.M. Elias, Epidermal lipids, membranes, and keratinization, Int. J. Dermatol. 20 (1981) 1–19. http://dx.doi.org/10.1111/j.1365-4362.1981.tb05278.x.
[2] J. van Smeden, L. Hoppel, R. van der Heijden, T. Hankemeier, R.J. Vreeken, J.A. Bouwstra, LC/MS analysis of stratum corneum lipids: ceramide profiling and discovery, J. Lipid Res. 52 (2011) 1211–1221. http://dx.doi.org/10.1194/jlr.M014456.
[3] B. Breiden, K. Sandhoff, The role of sphingolipid metabolism in cutaneous permeabilitybarrier formation, Biochim. Biophys. Acta Mol. Cell Biol. Lipids 1841 (2014) 441–452.
[4] Y. Uchida, W.M. Holleran, Omega-O-acylceramide, a lipid essential for mammalian survival, J. Dermatol. Sci. 51 (2008) 77–87. http://dx.doi.org/10.1016/j.jdermsci.2008.01.002.
[5] R. Sandhoff, Very long chain sphingolipids: tissue expression, function and synthesis, FEBS Lett. 584 (2010) 1907–1913. http://dx.doi.org/10.1016/j.febslet.2009.12.032.
[6] S. Motta, S. Sesana, R. Ghidoni, M. Monti, Content of the different lipid classes in psoriatic scale, Arch. Dermatol. Res. 287 (1995) 691–694. http://dx.doi.org/10.1007/BF00371745.
[7] J.A. Bouwstra, G.S. Gooris, F.E.R. Dubbelaar, A.M. Weerheim, A.P. IJzerman, M. Ponec, Role of ceramide 1 in the molecular organization of the stratum corneum lipids, J. Lipid Res. 39 (1998) 186–196.
[8] T.J. McIntosh, M.E. Stewart, D.T. Downing, X-ray diffraction analysis of isolated skin lipids: reconstitution of intercellular lipid domains†, Biochemistry (Mosc.) 35 (1996) 3649–3653. http://dx.doi.org/10.1021/bi952762q.
[9] J.A. Bouwstra, F.E. Dubbelaar, G.S. Gooris, M. Ponec, The lipid organisation in the skin barrier, Acta Derm. Venereol. Suppl. (Stockh.) 208 (2000) 23–30. http://dx.doi.org/10.1080/000155500750042826.
[10] P.M. Elias, J. Goerke, D.S. Friend, Mammalian epidermal barrier layer lipids: composition and influence on structure, J. Invest. Dermatol. 69 (1977) 535–546. http://dx.doi.org/10.1111/1523-1747.ep12687968.
[11] K.C. Madison, D.C. Swartzendruber, P.W. Wertz, D.T. Downing, Presence of intact intercellular lipid lamellae in the upper layers of the stratum corneum, J. Invest. Dermatol. 88 (1987) 714–718. http://dx.doi.org/10.1111/1523-1747.ep12470386.
[12] S.H. White, D. Mirejovsky, G.I. King, Structure of lamellar lipid domains and corneocyte envelopes of murine stratum corneum. An X-ray diffraction study, Biochemistry (Mosc.) 27 (1988) 3725–3732. http://dx.doi.org/10.1021/bi00410a031.
[13] L. Landmann, The epidermal permeability barrier. Comparison between in vivo and in vitro lipid structures, Eur. J. Cell Biol. 33 (1984) 258–264.
[14] M.A. Lampe, M.L. Williams, P.M. Elias, Human epidermal lipids: characterization and modulations during differentiation, J. Lipid Res. 24 (1983) 131–140.
[15] M.A. Lampe, A.L. Burlingame, J. Whitney, M.L. Williams, B.E. Brown, E. Roitman, et al., Human stratum corneum lipids: characterization and regional variations, J. Lipid Res. 24 (1983) 120–130.
[16] M. Schmuth, M.Q. Man, F. Weber, W. Gao, K.R. Feingold, P. Fritsch, et al., Permeability barrier disorder in Niemann–Pick disease: sphingomyelin–ceramide processing required for normal barrier homeostasis, J. Invest. Dermatol. 115 (2000) 459–466. http://dx.doi.org/10.1046/j.1523-1747.2000.00081.x.
[17] J.-M. Jensen, R. Fölster-Holst, A. Baranowsky, M. Schunck, S. Winoto-Morbach, C. Neumann, et al., Impaired sphingomyelinase activity and epidermal differentiation in atopic dermatitis, J. Invest. Dermatol. 122 (2004) 1423–1431. http://dx.doi.org/10.1111/j.0022-202X.2004.22621.x.
[18] S. Kusuda, C. Chang-Yi, M. Takahashi, T. Tezuka, Localization of sphingomyelinase in lesional skin of atopic dermatitis patients, J. Invest. Dermatol. 111 (1998) 733–738. http://dx.doi.org/10.1046/j.1523-1747.1998.00370.x.
[19] Y. Murata, J. Ogata, Y. Higaki, M. Kawashima, Y. Yada, K. Higuchi, et al., Abnormal expression of sphingomyelin acylase in atopic dermatitis: an etiologic factor for ceramide deficiency? J. Invest. Dermatol. 106 (1996) 1242–1249. http://dx.doi.org/10.1111/1523-1747.ep12348937.
[20] R. Okamoto, J. Arikawa, M. Ishibashi, M. Kawashima, Y. Takagi, G. Imokawa, Sphingosylphosphorylcholine is upregulated in the stratum corneum of patients with atopic dermatitis, J. Lipid Res. 44 (2003) 93–102. http://dx.doi.org/10.1194/jlr.M200225-JLR200.
[21] Y. Takagi, H. Nakagawa, T. Yaginuma, Y. Takema, G. Imokawa, An accumulation of glucosylceramide in the stratum corneum due to attenuated activity of beta-glucocerebrosidase is associated with the early phase of UVB-induced alteration in cutaneous barrier function, Arch. Dermatol. Res. 297 (2005) 18–25. http://dx.doi.org/10.1007/s00403-005-0567-7.
[22] J. Novotný, B. Janůšová, M. Novotný, A. Hrabálek, K. Vávrová, Short-chain ceramides decrease skin barrier properties, Skin Pharmacol. Physiol. 22 (2009) 22–30. http://dx.doi.org/10.1159/000183923.
[23] A.M. Kligman, E. Christophers, Preparation of isolated sheets of human stratum corneum, Arch. Dermatol. 88 (1963) 702–705. http://dx.doi.org/10.1001/archderm.1963.01590240026005.

[24] E.G. Bligh, W.J. Dyer, A rapid method of total lipid extraction and purification, Can. J. Biochem. Physiol. 37 (1959) 911–917. http://dx.doi.org/10.1139/o59-099.
[25] J.A. Bouwstra, G.S. Gooris, K. Cheng, A. Weerheim, W. Bras, M. Ponec, Phase behavior of isolated skin lipids, J. Lipid Res. 37 (1996) 999–1011.
[26] O. Bleck, D. Abeck, J. Ring, U. Hoppe, J.-P. Vietzke, R. Wolber, et al., Two ceramide subfractions detectable in Cer(AS) position by HPTLC in skin surface lipids of non-lesional skin of atopic eczema, J. Invest. Dermatol. 113 (1999) 894–900. http://dx.doi.org/10.1046/j.1523-1747.1999.00809.x.
[27] K. Vávrová, D. Henkes, K. Strüver, M. Sochorová, B. Školová, M.Y. Witting, et al., Filaggrin deficiency leads to impaired lipid profile and altered acidification pathways in a 3D skin construct, J. Invest. Dermatol. 134 (2013) 746–753. http://dx.doi.org/10.1038/jid.2013.402.
[28] D. Groen, G.S. Gooris, J.A. Bouwstra, Model membranes prepared with ceramide EOS, cholesterol and free fatty acids form a unique lamellar phase, Langmuir 26 (2010) 4168–4175. http://dx.doi.org/10.1021/la9047038.
[29] B. Školová, B. Janůšová, J. Zbytovská, G. Gooris, J. Bouwstra, P. Slepička, et al., Ceramides in the skin lipid membranes: length matters, Langmuir 29 (2013) 15624–15633. http://dx.doi.org/10.1021/la4037474.
[30] K. De Paepe, E. Houben, R. Adam, F. Wiesemann, V. Rogiers, Validation of the VapoMeter, a closed unventilated chamber system to assess transepidermal water loss vs. the open chamber Tewameter(r), Skin Res. Technol. 11 (2005) 61–69.
[31] W.J. Fasano, P.M. Hinderliter, The Tinsley LCR Databridge Model 6401 and electrical impedance measurements to evaluate skin integrity in vitro, Toxicol. In Vitro 18 (2004) 725–729. http://dx.doi.org/10.1016/j.tiv.2004.01.003.
[32] R.M. Fish, L.A. Geddes, C.F. Babbs, Medical and Bioengineering Aspects of Electrical Injuries, Lawyers & Judges Publishing Company, 2003.
[33] E.A. White, M.E. Orazem, A.L. Bunge, A critical analysis of single-frequency LCR databridge impedance measurements of human skin, Toxicol. In Vitro 25 (2011) 774–784. http://dx.doi.org/10.1016/j.tiv.2011.01.013.
[34] W. Abraham, D.T. Downing, Preparation of model membranes for skin permeability studies using stratum corneum lipids, J. Invest. Dermatol. 93 (1989) 809–813. http://dx.doi.org/10.1111/1523-1747.ep12284431.
[35] S. Mitragotri, Modeling skin permeability to hydrophilic and hydrophobic solutes based on four permeation pathways, J. Control. Release Off. J. Control. Release Soc. 86 (2003) 69–92. http://dx.doi.org/10.1016/S0168-3659(02)00321-8.
[36] S. Motta, M. Monti, S. Sesana, L. Mellesi, R. Ghidoni, R. Caputo, Abnormality of water barrier function in psoriasis: role of ceramide fractions, Arch. Dermatol. 130 (1994) 452–456. http://dx.doi.org/10.1001/archderm.1994.01690040056007.
[37] F. Netzlaff, K.-H. Kostka, C.-M. Lehr, U.F. Schaefer, TEWL measurements as a routine method for evaluating the integrity of epidermis sheets in static Franz type diffusion cells in vitro. Limitations shown by transport data testing, Eur. J. Pharm. Biopharm. 63 (2006) 44–50.
[38] J. Fokuhl, C.C. Müller-Goymann, Modified TEWL in vitro measurements on transdermal patches with different additives with regard to water vapour permeability kinetics, Int. J. Pharm. 444 (2013) 89–95. http://dx.doi.org/10.1016/j.ijpharm.2013.01.035.
[39] R.P. Chilcott, C.H. Dalton, A.J. Emmanuel, C.E. Allen, S.T. Bradley, Transepidermal water loss does not correlate with skin barrier function in vitro, J. Invest. Dermatol. 118 (2002) 871–875. http://dx.doi.org/10.1046/j.1523-1747.2002.01760.x.
[40] K. Vávrová, A. Hrabálek, S. Mac-Mary, P. Humbert, P. Muret, Ceramide analogue 14S24 selectively recovers perturbed human skin barrier, Br. J. Dermatol. 157 (2007) 704–712. http://dx.doi.org/10.1111/j.1365-2133.2007.08113.x.
[41] Y. Masukawa, H. Narita, H. Sato, A. Naoe, N. Kondo, Y. Sugai, et al., Comprehensive quantification of ceramide species in human stratum corneum, J. Lipid Res. 50 (2009) 1708–1719. http://dx.doi.org/10.1194/jlr.D800055-JLR200.
[42] B.M. Craven, Crystal structure of cholesterol monohydrate, Nature 260 (1976) 727–729. http://dx.doi.org/10.1038/260727a0.
[43] J.A. Bouwstra, G.S. Gooris, M.A.S. Vries, J.A. van der Spek, W. Bras, Structure of human stratum corneum as a function of temperature and hydration: a wide-angle X-ray diffraction study, Int. J. Pharm. 84 (1992) 205–216. http://dx.doi.org/10.1016/0378-5173(92)90158-X.
[44] M.W. de Jager, G.S. Gooris, I.P. Dolbnya, W. Bras, M. Ponec, J.A. Bouwstra, The phase behaviour of skin lipid mixtures based on synthetic ceramides, Chem. Phys. Lipids 124 (2003) 123–134. http://dx.doi.org/10.1016/S0009-3084(03)00050-1.
[45] D. Uhríková, G. Rapp, P. Balgavý, Condensed lamellar phase in ternary DNA-DLPC-cationic Gemini surfactant system: a small-angle synchrotron X-ray diffraction study, Bioelectrochemistry 58 (2002) 87–95. http://dx.doi.org/10.1016/S1567-5394(02)00122-6.
[46] J.A. Bouwstra, G.S. Gooris, J.A. van der Spek, W. Bras, Structural investigations of human stratum corneum by small-angle x-ray scattering, J. Invest. Dermatol. 97 (1991) 1005–1012. http://dx.doi.org/10.1111/1523-1747.ep12492217.
[47] J.A. Bouwstra, M. Ponec, The skin barrier in healthy and diseased state, Biochim. Biophys. Acta 1758 (2006) 2080–2095. http://dx.doi.org/10.1016/j.bbamem.2006.06.021.
[48] J.-M. Jensen, S. Schütze, M. Förl, M. Krönke, E. Proksch, Roles for tumor necrosis factor receptor p55 and sphingomyelinase in repairing the cutaneous permeability barrier, J. Clin. Invest. 104 (1999) 1761–1770. http://dx.doi.org/10.1172/JCI5307.
[49] T. Yamamura, T. Tezuka, Change in sphingomyelinase activity in human epidermis during aging, J. Dermatol. Sci. 1 (1990) 79–83. http://dx.doi.org/10.1016/0923-1811(90)90219-4.
[50] J.-M. Jensen, M. Förl, S. Winoto-Morbach, S. Seite, M. Schunck, E. Proksch, et al., Acid and neutral sphingomyelinase, ceramide synthase, and acid ceramidase activities in cutaneous aging, Exp. Dermatol. 14 (2005) 609–618. http://dx.doi.org/10.1111/j.0906-6705.2005.00342.x.
[51] P.R. Cullis, M.J. Hope, The bilayer stabilizing role of sphingomyelin in the presence of cholesterol: a 31P NMR study, Biochim. Biophys. Acta 597 (1980) 533–542.
[52] W.G. Hill, M.L. Zeidel, Reconstituting the barrier properties of a water-tight epithelial membrane by design of leaflet-specific liposomes, J. Biol. Chem. 275 (2000) 30176–30185. http://dx.doi.org/10.1074/jbc.M003494200.
[53] R. Fettiplace, The influence of the lipid on the water permeability of artificial membranes, Biochim. Biophys. Acta 513 (1978) 1–10.
[54] R. Hertz, Y. Barenholz, Permeability and integrity properties of lecithin–sphingomyelin liposomes, Chem. Phys. Lipids 15 (1975) 138–156. http://dx.doi.org/10.1016/0009-3084(75)90037-7.
[55] J.P. Slotte, Biological functions of sphingomyelins, Prog. Lipid Res. 52 (2013) 424–437. http://dx.doi.org/10.1016/j.plipres.2013.05.001.
[56] L.R. Montes, M.B. Ruiz-Argüello, F.M. Goñi, A. Alonso, Membrane restructuring via ceramide results in enhanced solute efflux, J. Biol. Chem. 277 (2002) 11788–11794. http://dx.doi.org/10.1074/jbc.M111568200.
[57] G.G. Shipley, L.S. Avecilla, D.M. Small, Phase behavior and structure of aqueous dispersions of sphingomyelin, J. Lipid Res. 15 (1974) 124–131.
[58] B. Steinbauer, T. Mehnert, K. Beyer, Hydration and lateral organization in phospholipid bilayers containing sphingomyelin: a 2H-NMR study, Biophys. J. 85 (2003) 1013–1024. http://dx.doi.org/10.1016/S0006-3495(03)74540-8.
[59] C. Faure, J.-F. Tranchant, E.J. Dufourc, Interfacial hydration of ceramide in stratum corneum model membrane measured by ^2H NMR of D_2O, J. Chim. Phys. Phys. Chim. Biol. 95 (1998) 480–486. http://dx.doi.org/10.1051/jcp:1998163.
[60] D. Vaknin, M.S. Kelley, The structure of D-erythro-C18 ceramide at the air–water interface, Biophys. J. 79 (2000) 2616–2623. http://dx.doi.org/10.1016/S0006-3495(00)76500-3.
[61] J. Rautio, Prodrugs and Targeted Delivery: Towards Better ADME Properties, John Wiley & Sons, 2011.
[62] T.J. McIntosh, S.A. Simon, D. Needham, C.H. Huang, Structure and cohesive properties of sphingomyelin/cholesterol bilayers, Biochemistry (Mosc.) 31 (1992) 2012–2020. http://dx.doi.org/10.1021/bi00122a017.
[63] K.P. Shaw, N.J. Brooks, J.A. Clarke, O. Ces, J.M. Seddon, R.V. Law, Pressure–temperature phase behaviour of natural sphingomyelin extracts, Soft Matter 8 (2012) 1070–1078. http://dx.doi.org/10.1039/C1SM06703F.
[64] W. Rawicz, K.C. Olbrich, T. McIntosh, D. Needham, E. Evans, Effect of chain length and unsaturation on elasticity of lipid bilayers, Biophys. J. 79 (2000) 328–339. http://dx.doi.org/10.1016/S0006-3495(00)76295-3.
[65] T.J. McIntosh, The effect of cholesterol on the structure of phosphatidylcholine bilayers, Biochim. Biophys. Acta 513 (1978) 43–58.
[66] C.L. Gay, R.H. Guy, G.M. Golden, V.H.W. Mak, M.L. Francoeur, Characterization of low-temperature (i.e., <65 °C) lipid transitions in human stratum corneum, J. Invest. Dermatol. 103 (1994) 233–239.
[67] F. Damien, M. Boncheva, The extent of orthorhombic lipid phases in the stratum corneum determines the barrier efficiency of human skin in vivo, J. Invest. Dermatol. 130 (2009) 611–614. http://dx.doi.org/10.1038/jid.2009.272.
[68] D. Groen, D.S. Poole, G.S. Gooris, J.A. Bouwstra, Is an orthorhombic lateral packing and a proper lamellar organization important for the skin barrier function? Biochim. Biophys. Acta 1808 (2011) 1529–1537. http://dx.doi.org/10.1016/j.bbamem.2010.10.015.
[69] Y. Barenholz, T.E. Thompson, Sphingomyelins in bilayers and biological membranes, Biochim. Biophys. Acta Rev. Biomembr. 604 (1980) 129–158. http://dx.doi.org/10.1016/0304-4157(80)90006-4.
[70] M. Mao-Qiang, M. Jain, K.R. Feingold, P.M. Elias, Secretory phospholipase A2 activity is required for permeability barrier homeostasis, J. Invest. Dermatol. 106 (1996) 57–63.
[71] A.W. Eliasz, D. Chapman, D.F. Ewing, Phospholipid phase transitions. Effects of n-alcohols, n-monocarboxylic acids, phenylalkyl alcohols and quatenary ammonium compounds, Biochim. Biophys. Acta Biomembr. 448 (1976) 220–233. http://dx.doi.org/10.1016/0005-2736(76)90238-8.
[72] G.H. Peters, F.Y. Hansen, M.S. Møller, P. Westh, Effects of fatty acid inclusion in a DMPC bilayer membrane, J. Phys. Chem. B 113 (2009) 92–102. http://dx.doi.org/10.1021/jp806205m.
[73] I. Iwai, H. Han, L. den Hollander, S. Svensson, L.-G. Ofverstedt, J. Anwar, et al., The human skin barrier is organized as stacked bilayers of fully extended ceramides with cholesterol molecules associated with the ceramide sphingoid moiety, J. Invest. Dermatol. 132 (2012) 2215–2225. http://dx.doi.org/10.1038/jid.2012.43.
[74] R.W. Corkery, The anti-parallel, extended or splayed-chain conformation of amphiphilic lipids, Colloids Surf. B Biointerfaces 26 (2002) 3–20. http://dx.doi.org/10.1016/S0927-7765(02)00034-6.
[75] T.J. McIntosh, Organization of skin stratum corneum extracellular lamellae: diffraction evidence for asymmetric distribution of cholesterol, Biophys. J. 85 (2003) 1675–1681. http://dx.doi.org/10.1016/S0006-3495(03)74597-4.
[76] K.S. Bruzik, Conformation of the polar headgroup of sphingomyelin and its analogues, Biochim. Biophys. Acta 939 (1988) 315–326.
[77] I. Pascher, S. Sundell, Molecular arrangements in sphingolipids. The crystal structure of cerebroside, Chem. Phys. Lipids 20 (1977) 175–191.